



This is a repository copy of *Magnetic-Silk Core–Shell Nanoparticles as Potential Carriers for Targeted Delivery of Curcumin into Human Breast Cancer Cells*.

White Rose Research Online URL for this paper:
<http://eprints.whiterose.ac.uk/118277/>

Version: Accepted Version

Article:

Song, W., Muthana, M. orcid.org/0000-0003-2497-8903, Mukherjee, J. et al. (3 more authors) (2017) Magnetic-Silk Core–Shell Nanoparticles as Potential Carriers for Targeted Delivery of Curcumin into Human Breast Cancer Cells. *ACS Biomaterials Science & Engineering*, 3 (6). pp. 1027-1038. ISSN 2373-9878

<https://doi.org/10.1021/acsbomaterials.7b00153>

Reuse

Items deposited in White Rose Research Online are protected by copyright, with all rights reserved unless indicated otherwise. They may be downloaded and/or printed for private study, or other acts as permitted by national copyright laws. The publisher or other rights holders may allow further reproduction and re-use of the full text version. This is indicated by the licence information on the White Rose Research Online record for the item.

Takedown

If you consider content in White Rose Research Online to be in breach of UK law, please notify us by emailing eprints@whiterose.ac.uk including the URL of the record and the reason for the withdrawal request.



eprints@whiterose.ac.uk
<https://eprints.whiterose.ac.uk/>

Magnetic-Silk Core-Shell Nanoparticles as Potential Carriers for Targeted Delivery of Curcumin into Human Breast Cancer Cells

Wenxing Song¹, Munita Muthana², Joy Mukherjee¹, Robert J. Falconer¹, Catherine A. Biggs¹, Xiubo Zhao^{1*}

¹Department of Chemical and Biological Engineering, University of Sheffield, Mappin Street, Sheffield S1 3JD, UK

²Departments of Infection and Immunity, University of Sheffield, Beech Hill Road, Sheffield S10 2RX, UK

*Author for correspondence: Xiubo Zhao, phone +44 114 222 8256, email:

Xiubo.zhao@sheffield.ac.uk

Abstract

Curcumin is a promising anti-cancer drug but its applications in cancer therapy are limited due to its poor solubility, short half-life and low bioavailability. In this paper, we present a curcumin loaded magnetic silk fibroin core-shell nanoparticle system for sustained release of curcumin into breast cancer cells. Curcumin loaded magnetic silk fibroin core-shell nanoparticles were fabricated by a simple salting-out method using sodium phosphate with magnetic nanoparticles. The size, zeta potential, encapsulation/ loading efficiency and curcumin release rate were controlled and optimised by regulating silk fibroin concentration, pH value of the phosphate solution and curcumin usage. Curcumin loaded magnetic silk fibroin core-shell nanoparticles showed enhanced cytotoxicity and higher cellular uptake in the human Caucasian breast adenocarcinoma cell line (MDA-MB-231 cells) evidenced by MTT and cellular uptake assays. In addition, silk fibroin nanoparticles and magnetic silk fibroin nanoparticles without curcumin loaded were used as controls. The particles prepared using sodium phosphate showed significantly smaller diameter (90-350 nm) compared with those prepared using potassium phosphate, which possess a diameter range of 500-1200 nm. These smaller particles are superior for biomedical applications since such size range is particularly desired for cell internalization. In addition, the magnetic cores inside the particles provide possibility of using an external magnet for cancer targeting.

Keywords: Silk, Magnetic nanoparticles, Drug delivery, Cancer, Curcumin

1. Introduction

Curcumin (CUR) is the main component of turmeric which is extracted from the root of *Curcuma longa* native to Southeast Asia ¹. It is considered a pharmacologically safe drug ² and has been widely used in medicine due to its anti-oxidant ³⁻⁵ anti-inflammatory ⁶⁻⁸ wound healing ⁹⁻¹⁰ and anti-bacterial ¹¹⁻¹² properties. Also, CUR has been widely used to fight against cisplatin-resistant cancer cells and decrease its unwanted side effects ¹³. Moreover, it has also been found that CUR may modulate markers of High-density lipoprotein (HDL) function and subsequently improve conditions in which HDL is dysfunctional ¹⁴. Recent research revealed that CUR also possess anti-cancer properties on multiple cell lines via its effects on the regulation of cellular growth and apoptosis ¹⁵⁻¹⁷ which makes it a promising drug for cancer therapy. However, due to its poor solubility in aqueous solution ¹⁸⁻¹⁹, short half-life in the body and low bioavailability after oral administration ²⁰⁻²², the accumulation and uptake of CUR at the disease area by itself is very poor. Therefore, the applications of CUR as an anti-cancer drug have been significantly limited ^{19-21,23}. To overcome these obstacles, various strategies including the development of liposome ²⁴, phospholipid ²⁵, adjuvants ²⁶ and nanoparticle carriers ²⁷ for CUR delivery have been conducted. However, most of these drug delivery systems lack the ability of tumour targeting, which makes the accumulation of drugs at tumour sites limited. Thus, a drug delivery system which is capable of not only improving the availability, cell uptake and half-life of CUR, but can also deliver it to disease sites is desired. In this report, we present the fabrication of CUR loaded magnetic silk fibroin core-shell nanoparticles (CMSPs) for the delivery of CUR into breast cancer cells.

Silk fibroin (SF) protein from cocoons of *Bombyx mori* is an FDA approved, natural derived material and has been widely used to form various biomaterials including SF gels, sponges and films for different medical applications ²⁸. It has also been demonstrated that SF is an extremely promising material for drug delivery systems due to its excellent biocompatibility ²⁹, tunable biodegradability ³⁰ and easy processing ²⁸. An increasing number of strategies including capillary-microdot technique ³¹, desolvation method ³²⁻³⁵, supercritical fluid technologies ³⁶ and salting-out method ³⁷ have been developed to fabricate SF based nanoparticles that can load and release model drugs. For example,

Gupta *et al.* have fabricated CUR loaded SF nanoparticles (<100 nm) with the capillary-microdot technique ³¹. However, preparation of SF nanoparticles (SFPs) with this method is difficult to process and the yield is relatively low. Kundu *et al.* have prepared SFPs (150 -170 nm) with the desolvation method by adding SF solutions into dimethyl sulfoxide (DMSO) ³². Nevertheless, the organic solvent residue in these SFPs is still difficult to avoid. Zhao *et al.* ³⁶ have prepared smaller SFPs (~ 50 nm) using solution-enhanced dispersion by CO₂. However, the processing of this method is complicated and the cost is high. Lammel *et al.* have developed a salting-out method for the preparation of SFPs (500 -1200 nm) by adding SF solution into potassium phosphate solutions ³⁷. This method possesses several advantages such as low cost, simplicity and safe operation, avoiding the use of toxic solvents and easy to maintain protein activities. However, the size of SF particles prepared with this approach is relatively large, which means their circulation time in blood will be shorter and are more likely to be entrapped within the liver and spleen ³⁸.

Targeted drug delivery using magnetic carriers with an external magnetic field focused on the tumour areas has been reported as a promising strategy. This strategy possesses advantages such as visualize the targeting process, rapid targeting and potential of being heated in a magnetic field to promote drug release as well as avoiding complicated chemical modification of targeting ligands on the surface of nanocarriers³⁹. Therefore, the combination of magnetic nanoparticles (MNPs) and SF become a promising strategy for targeted drug delivery. Recently, Shao and co-workers successfully prepared Doxorubicin (DOX) loaded magnetic silk fibroin nanoparticles (DMSPs) using the potassium phosphate salting-out method ⁴⁰. The as-prepared DMSPs were proved capable of delivering the drug to the tumour site with the help of an external magnetic field. Nevertheless, targeted delivery of CUR using magnetic silk fibroin particles (MSPs), and the use of sodium phosphate to make smaller SFPs, to the best of our knowledge, has not yet been reported. It has been observed in our result that SFPs fabricated using sodium phosphate possess much smaller particle sizes (90 – 300 nm) compared with those fabricated with potassium phosphate, which normally possess the size over 500 nm. Since the particle size and performance of SFPs produced using sodium phosphate is significantly different from those fabricated using potassium phosphate and the properties of these particles have not yet been studied. It is important to investigate the size, zeta potential, secondary structure, CUR loading/ release efficiency of SFPs and CMSPs prepared using sodium phosphate. On the other hand, it is expected that CUR will easily encapsulated or

adsorbed on the water-insoluble SFPs or CMSPs due to the strong hydrophobic interaction between hydrophobic CUR and the water-insoluble silk-II structure formed during the salting-out process. High encapsulation and loading efficiency of CUR in SFPs and CMSPs are also expectable, which is desired for a drug delivery system. Therefore, in this paper, we prepared CMSPs with the salting-out method using sodium phosphate instead of potassium phosphate to prepare smaller SFPs. The particle properties including size, zeta potential and CUR loading/release efficiency were investigated. In addition, how processing parameters such as pH value of sodium phosphate solution affect those properties were also studied. The cytotoxicity and cellular uptake performance of CMSPs was investigated using MDA-MB-231 (human breast adenocarcinoma) cells.

2. Materials and methods

2.1. Materials

Bombyx mori silk was obtained from Jiangsu, R.P. China. Na₂CO₃ (11552) was purchased from Alfa Aesar. Curcumin (C8069) was purchased from LKT Laboratories. Paraformaldehyde (sc-253236A) was purchased from Chem Cruz®. K₂HPO₄ (BP363), KH₂PO₄ (BP362), CaCl₂ (C1016), Na₂HPO₄ (S7907), NaH₂PO₄ (S8282), FeCl₂ (44939), FeCl₃ (44944), ammonium hydroxide (221228) DMSO (Dimethyl sulfoxide, D5879) and Rhodamine B isothiocyanate (R1755) were purchased from SIGMA-ALDRICH. Roswell Park Memorial Institute (RPMI) 1640 Medium (BE 12-167F), PBS (Dulbecco's Phosphate Buffered Saline, BE17-512F), Penicillin 5.000 U/ml-Streptomycin 5.000 U/ml (DE17-603E), Foetal Bovine Serum (FBS), L-Glutamine (17-605F) were purchased from Lonza®. Texas Red®-X Phalloidin (T7471), MTT (M6494) assay and DAPI (4', 6-Diamidino-2-phenylindole dihydrochloride, D1306) were purchased from Thermo Fisher Scientific. MDA-MB-231 cells (Human Caucasian Breast Adenocarcinoma cells) were purchased from ECACC. Ultra-High Quality (UHQ) water was prepared using PURELAB Classic (ELGA).

2.2. Preparation of silk fibroin solution

Silk was boiled in 0.02 M Na₂CO₃ solution for 30 min before rinsed 3 to 4 times with UHQ water to remove sericin. After drying overnight, the degummed fibroin was dissolved in a ternary system

(CaCl₂/ Ethanol/ water = 1: 2: 8 molar ratio) at 75 °C for 3 h before dialysed in a cellulose tube (molecular weight cut off 12 kDa) against UHQ water for 3 days to remove the remaining CaCl₂. Finally, the SF solution was centrifuged twice (10,000 rpm) and filtered with 0.45 µm filter to remove the impurities. The regenerated silk fibroin (RSF) aqueous solution was stored in the refrigerator at 4 °C.

2.3. Preparation of magnetic nanoparticles

In brief, 4 g FeCl₃ and 4.5 g FeCl₂ were dissolved in 300 ml UHQ water and then the mixture was placed in a 500 ml round-bottom flask for 30 min with a nitrogen purge to replace the air in the flask. 15 ml ammonium hydroxide was then added to the blend with vigorous stirring under nitrogen atmosphere at room temperature for 2 h. The MNPs were washed 5 times and collected using Neodymium magnets. The particles were dried over night at room temperature and stored for future usage.

2.4. Preparation of silk fibroin particles and magnetic silk fibroin particles

2.4.1. Silk fibroin particles preparation

Briefly, SF solutions with different concentrations (0.1 - 12 mg/ml) were added to potassium phosphate or sodium phosphate solutions (ionic strength: 1.25 M, pH 8) in a volume ratio of 1:5 followed by storing the as-prepared mixtures in the refrigerator for 2 h at -20 °C. The resulting particles were unfrozen and centrifuged at 20,000 g for 15 min before being re-dispersed and washed three times in UHQ water. To investigate the effect of phosphate ionic strength on SF particle size, sodium/ potassium phosphate solutions with ionic strength from 0.6 to 2 M were mixed with SF solutions (5 mg/ml). The effect of sodium phosphate pH on the secondary structure of SF particles was also studied by producing SFPs with sodium phosphate solutions at pH 4, 7 and 9. Secondary structures of SFPs were investigated with Fourier transform infrared (FTIR) spectroscopy.

2.4.2. Magnetic silk fibroin particles preparation

MNPs were dispersed in sodium phosphate (1.25 M, pH 8) solution to reach the concentration of 0.1 mg/ml. The MNP-salt mixture was then blended with SF (0.5 - 10 mg/ml) solutions to produce particles according to the process mentioned in section 2.4.1 and the resulting MSPs were collected

using Neodymium magnets. Sodium phosphate solutions with different pH values were also mixed with SF solution (5 mg/ml) to investigate the effect of pH on MSP size.

2.5. Curcumin loaded magnetic silk fibroin particles

CUR was dissolved in DMSO with a concentration of 100 mg/ml CUR DMSO solution. 1 mg MNPs and different amount of CUR DMSO solutions (with CUR weight equal to 10%, 30%, 60% and 90% of total SF used) were added to 10 ml sodium phosphate (1.25 M, pH 8) solution. To investigate the effect of pH on CMSP size, zeta potential and CUR release rate, sodium phosphate solutions with pH value 4, 7, 8 and 9 were used (while the CUR usage was 10 %). The prepared mixture was then blended with 2 ml SF solution (5 mg/ml) and stored at -20 °C for 2h. The CMSPs were then unfrozen and the supernatant was analysed to determine residual CUR concentration using UV-Vis spectrometry (JENWAY 6715, Bibby Scientific, UK). Standard calibration curves for CUR in sodium phosphate and PBS were used. Concentration of particles was determined by weighing dried particles from 1 ml solution. Encapsulation and loading efficiencies were determined by equations (1) and (2) below:

$$\text{Encapsulation efficiency (w/w\%)} = \frac{\text{amount of CUR in particles}}{\text{CUR initially added}} \times 100\% \quad (1)$$

$$\text{Loading efficiency (w/w\%)} = \frac{\text{amount of CUR in particles}}{\text{amount of particles}} \times 100\% \quad (2)$$

2.6. Release of curcumin from curcumin loaded magnetic silk fibroin core-shell nanoparticles

5 mg of drug loaded CMSPs was washed with UHQ water and suspended in 5 ml PBS (pH 7.4) before incubated at 37 °C with shaking (200 rpm). The suspensions were centrifuged (10,000 g) every 24 h and the supernatants were carefully removed and replaced with fresh PBS. The CUR concentrations of these supernatant were analysed using UV-Vis-spectrometry and the percentage of cumulative CUR release was plotted as a function of incubation time.

2.7. Particle characterization

2.7.1. Dynamic light scattering and Zeta potential analysis

The size and Zeta potential of SFPs were measured using dynamic light scattering (DLS)

(NanoBrook 90 plus Pals Particle size Analyzer, Brookhaven Instrument, NY, USA). A diode laser with wavelength of 660 nm was used. The temperature was kept at 18 °C with a circulation bath. Refractive indexes of 1.331 for water and 1.540 for particles were employed for the calculation of particle size.

2.7.2. Fourier transform infrared spectroscopy

Fourier transform infrared spectroscopy (FTIR) analysis was conducted with Fourier Transform Infrared Spectrophotometer (IR Prestige-21, Shimadzu, UK). SFPs were washed three times with UHQ water and allowed to air dry on the diamond attenuated total reflectance (ATR) attachment (ATR apparatus, Pike Technologies, USA) of the spectrophotometer. The range of wave numbers was set from 400 to 4000 cm^{-1} and the spectrum was read using the Happ-Genzel apodisation function over 64 scans with a resolution of 4 cm^{-1} . The amide I region (1575 - 1750 cm^{-1}) was investigated to determine the secondary structure of SF protein. The spectral processing was conducted with the software IR solution provided within the FTIR instrument.

2.7.3. Atomic Force Microscopy analysis

Atomic Force Microscopy (AFM) (Dimension Icon with ScanAsyst, Bruker Corporation, U.S.A) was used to reveal the size and morphology of the particles. Particle solutions were dropped on mica substrates and air dried before putting on the sample stage, SCANASYST-AIR tip were used and the data was analysed with NanoScope Analysis 1.5 software.

2.7.4. Transmission electron microscopy analysis

Transmission electron microscopy (TEM) images were obtained using a Fei Tecnai BioTWIN 120 kV instrument. Operating voltage used was 80 kV. Images recorded using a Gatan Orius SC1000B bottom mounted digital camera and Gatan Digital Micrograph software.

2.8. *In vitro* cytotoxicity assay

MDA-MB-231 cells were cultured in RPMI medium supplemented with 10 % Foetal Bovine Serum (FBS), 1 % Penicillin / Streptomycin and 1 % L-Glutamine at 37 °C and 5 % CO_2 . The cytotoxicity of SFPs, MSPs and CMSPs against MDA-MB-231 cells was investigated by the MTT assay. The cells were seeded in 96 - well plates at a density of 5×10^3 cells per well before incubation for 24 h to allow cells to attach to the plates. Cells were then incubated with SFPs, MSPs, CMSPs (30 % CUR

usage) and free CUR (amount equal to the CUR content in CMSPs) at preselected concentrations respectively. After 3 days incubation, 50 μ l of 3 mg/ml MTT was added to each well and incubated at 37 °C for 3 h followed by removing the supernatants and adding 200 μ l DMSO. A plate reader (Thermo Scientific® Multiskan FC) was used to measure the absorbance of each well including control wells containing only medium at 540 nm. The relative cell viability was determined by comparing the absorbance with control wells.

2.9. Cellular uptake assays

SF was labelled with Rhodamine B isothiocyanate (Ex 543 nm, Em 580 nm) before used for the fabrication of SFPs, MSPs and CMSPs fabrication. MDA-MB-231 cells were seeded in 6 - well plates with 3×10^5 cells per well and incubated overnight at 37 °C and 5 % CO₂ before incubation with Rhodamine B labelled SFPs, MSPs and CMSPs (30% CUR usage) at particle concentrations in medium from 3 -100 μ g/ml. After 24 h, the cells were harvested with trypsin and washed twice with PBS to remove free particles. The intracellular fluorescence of Rhodamine B and CUR was determined using a flow cytometer (FACS Calibur, BD Biosciences, USA) to investigate the particle and CUR uptake.

To obtain microscopy images of cellular uptake, MDA-MB-231 cells were incubated on the cover slips in 12 - well plates at a concentration of 1×10^5 cells per well and incubated with CMSPs (30% CUR usage) at 37 °C and 5 % CO₂ for 3 h. Cells were washed three times with PBS to remove non-specifically adsorbed particles or CUR before fixation with 4 % paraformaldehyde at room temperature for 30 min. The fixed cells were stained with 3 μ l 1% Texas Red®-X Phalloidin (Ex 591 nm, Em 608 nm) for 1 h and washed twice with PBS followed by staining with DAPI (Ex 358 nm, Em 461 nm) for 30 min. Finally, cells washed twice with PBS ready for fluorescent microscope (AF6000, Leica, Germany). Fluorescent images of DAPI, Texas Red and CUR (Ex 340 nm, Em 530 nm⁴¹) stained cells were captured using different channels. All images were captured and analyzed with LAS AF Lite software (Leica).

3. Results

3.1. Controlling the size and secondary structures of silk fibroin nanoparticles

To investigate the effect of SF concentration and different salts on the size of SFP, SF solution with

various concentrations (0.1-12 mg/ml) were added to 1.25 M sodium or potassium phosphate (pH 8) solutions and kept at - 20 °C for 2 h. The as-prepared particles were measured with DLS. As shown in Fig.1a, when using potassium phosphate, increasing SF concentrations from 0.1 to 12 mg/ml, resulted in the change of particle mean diameter from 0.62 to 2.12 μm which is very similar to the result reported by Kaplan and co-workers³⁷. It is clear that SFPs fabricated with sodium phosphate showed much smaller sizes (90 - 300 nm) and narrower size distributions (Fig.1a) than those fabricated with potassium phosphate.

The effect of ionic strength on the size of the particles has also been investigated. Fig.1b illustrates the diameter of SFPs fabricated with sodium or potassium phosphate as a function of the ionic strength of the salts. Below 0.6 M ionic strength, particles in both salt solutions can hardly be detected. Therefore, it was assumed that the lowest ionic strength to form particles is 0.6 M. This finding is consistent with the literature³⁷. Increased ionic strength resulted in larger particles for both cases, which is assumed to be a result of enhanced denaturation of SF and aggregation of smaller SFPs. It is also clear that at the same ionic strength, particles fabricated with potassium phosphate are much larger than those fabricated with sodium phosphate. AFM images of SFPs fabricated by adding SF solution (12 mg/ml) into sodium or potassium phosphate solution (1.25 M, pH 8) are shown in Fig.1c-d. Particles formed using sodium phosphate are much smaller (380 nm) and smoother, while particles formed by potassium phosphate are larger (1800 nm) in size and have a rough surface that may result from the aggregation of smaller particles. Therefore, by using different phosphate solutions or adjusting their ionic strength, SFPs with a large range of diameters (90 nm- 2.2 μm) can be prepared, providing more options on designing SFPs for different applications.

The solution pH can also affect particle size. Fig.1e showed the diameter of SFPs fabricated with sodium phosphate as a function of pH, the ionic strength of solutions was fixed at 1.25 M. From pH 4 to 9, the size of particles decreased gradually. The isoelectric point (pI) of SF is 4.53³⁷, at which pH the net charge of SF is close to 0 and thus tend to aggregate due to the increased inter-molecular interaction³⁷. At pH higher than the pI, the net charges of SF are negative and the charge density tends to increase as pH increases. As a result, the increased repulsion resulted in smaller SFPs and prevented further aggregation.

To investigate the effect of pH values on SF secondary structures, FTIR analysis was carried out

and the results are shown in Fig.1f. Absorption band in the frequency range of 1616 - 1637 cm^{-1} represents the β -sheet rich silk-II form while those in the frequency range from 1636 - 1655 cm^{-1} represent the random coil rich silk-I form ⁴². The secondary structure contains more silk II structure, and is more hydrophobic, at pH 4 compared to a less hydrophobic silk I-rich structure at pH 9. These results explain the change on SFPs size at different pH values: more hydrophobic particles have larger tendency to gather and form bigger aggregates. Furthermore, this phenomenon is very useful in manipulating drug loading, for example, increasing the loading efficiency of hydrophobic drugs on particles by using more hydrophobic particles.

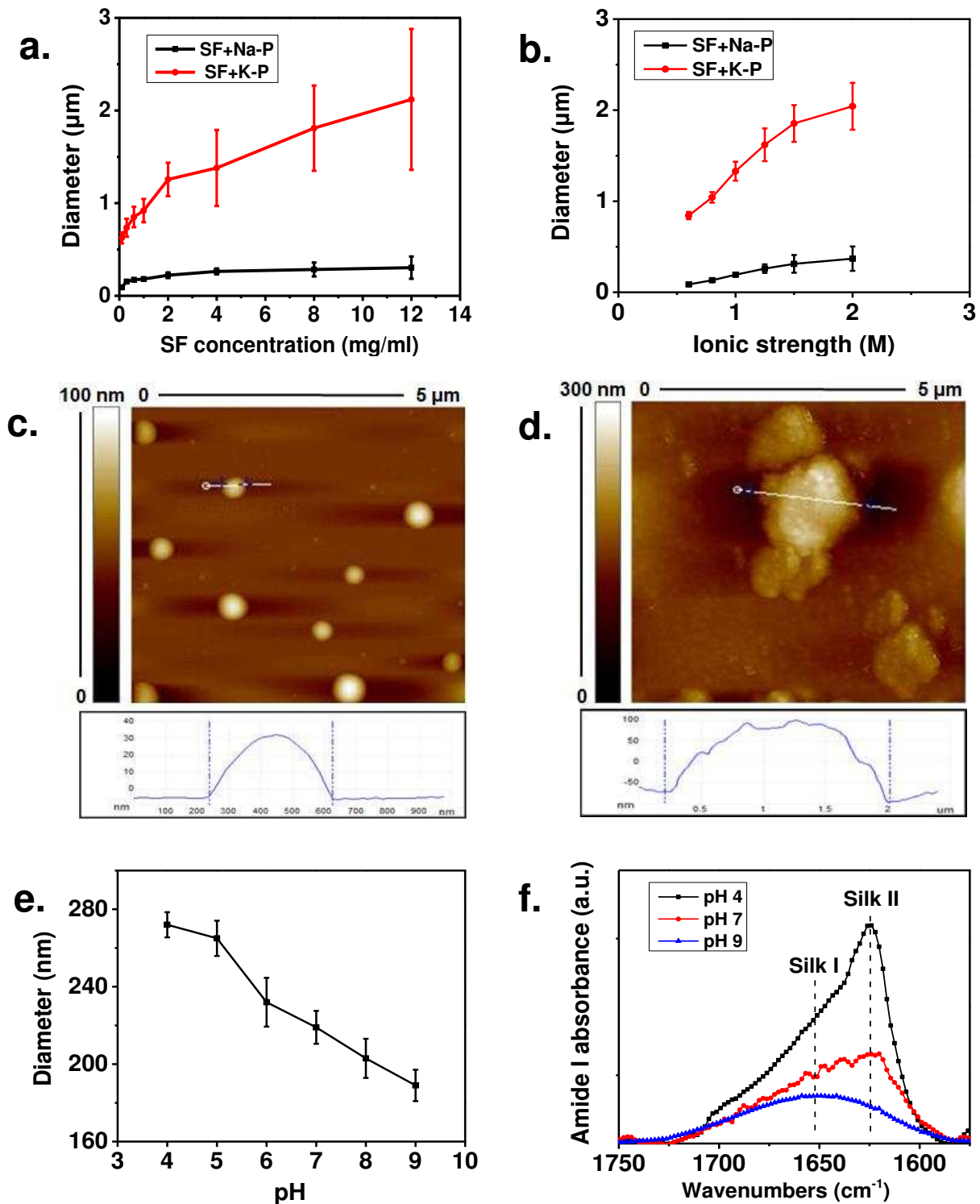


Fig.1. Effects of SF concentration, salt, ionic strength and solution pH to the particle size and protein secondary structure. a) Particle diameter as a function of SF concentration when adding SF solutions (concentration from 0.1-12 mg/ml) to sodium phosphate (Na-P) and potassium phosphate (K-P) solutions (both at ionic strength 1.25 M, pH 8) at the volume ratio of 1:5. b) Diameter of SFPs fabricated with K-P or Na-P as a function of their ionic strength. The SF concentration was fixed at 5

mg/ml. c-d) AFM images of particles fabricated by adding SF solution (12 mg/ml) in to sodium phosphate (c) and potassium phosphate (d). Both solutions are at the ionic strength of 1.25 M and pH 8. e) Diameter of SFPs fabricated with Na-P as a function of the pH of Na-P solutions. f) FTIR spectra of particles produced by salting-out by 1.25 M sodium phosphate at different pH values. The results are shown in mean \pm SD, $n \geq 3$. It was found from the above results that the use of sodium phosphate, lower ionic strength and higher pH of solution produces smaller SFPs.

3.2. Controlling the size and Zeta potential of magnetic silk fibroin nanoparticles and curcumin loaded magnetic silk fibroin core-shell nanoparticles

Magnetic Fe_3O_4 nanoparticles (MNPs) with diameter 10 - 30 nm were introduced to SFPs by adding MNPs into sodium phosphate solutions (1.25 M, pH 8) before mixed with SF solutions. As shown in Fig.2, as-prepared magnetic-SF core-shell particles (MSPs) can be rapidly collected with the help of an external magnetic force from a Neodymium magnet, which can be potentially used for the targeted delivery of particles to desired tissue sites⁴⁰.

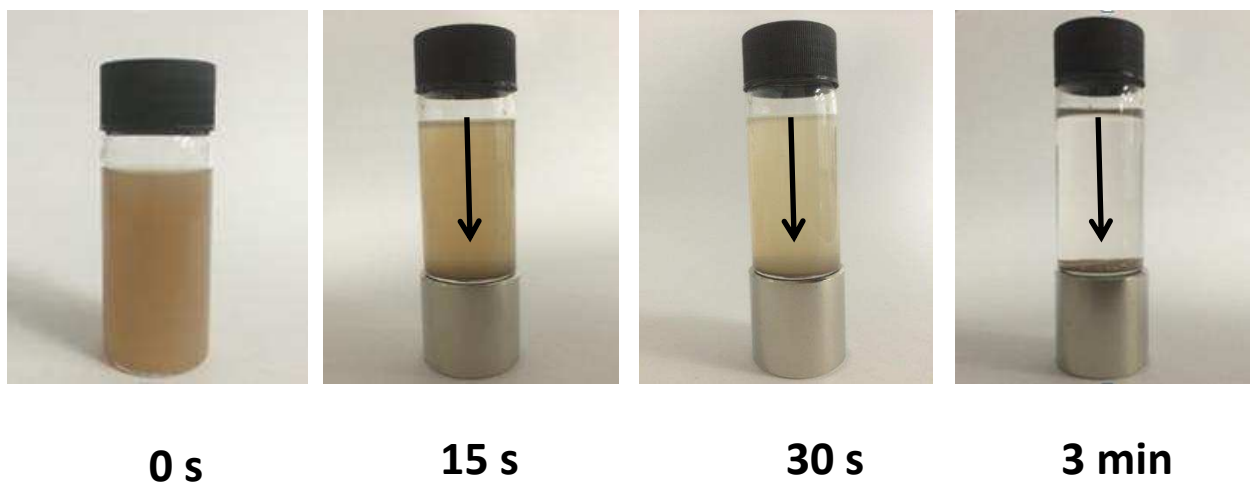


Fig.2. MSPs can be rapidly collected with a Neodymium magnet (pull force 25Kg, 25.4mm Diameter x 30 mm Thick) within 3 min.

The size of as-prepared MSPs can be manipulated by changing SF concentration or pH values of sodium phosphate used. Fig.3a illustrates the diameter of MSPs as a function of SF concentrations. The addition of MNPs did not change the particle size of SFPs. Instead, the particles size remained

within the range of 100 - 250 nm. This result is in agreement with the work of Tian *et al.* who have reported that, when using potassium phosphate, the addition of MNPs can dramatically decrease the particle size of SFPs from 1.4 μm to 130 - 210 nm⁴⁰. Fig.3b showed the effect of sodium phosphate pH on MSP diameter. It is clear that both SF concentration and sodium phosphate pH affect MSP size similarly as they affect SF particle size (Fig.1a&e), which suggests the property of MSPs is dominated by the SF structures coated on the MNPs.

CMSPs were fabricated by adding CUR and MNPs into sodium phosphate solution (1.25 M, pH 8) followed by adding SF solution (5 mg/ml) into the mixture. As shown in Fig.3c, increasing the amount of CUR (with weight equivalent to the percentages of the weight of SF used) resulted in the diameter increase of CMSPs, indicating the drug loading into the particles. The Zeta potential of the CMSPs with different CUR loading was measured. As shown in Fig.3e, higher CUR usages resulted in less charge densities, which lead to weaker repulsive interactions and therefore, larger particles. The same reason can also be used to explain the effect of pH value on CMSP size. As shown in Fig.3d, CMSP diameter decreases with the increase of sodium phosphate pH value. Meanwhile, Fig.3f illustrates that higher pH values correspond to higher charge densities. Thus, we may conclude that the property of CMSPs is also dominated by its SF content, therefore, higher pH value correspond to higher charge densities and smaller particles.

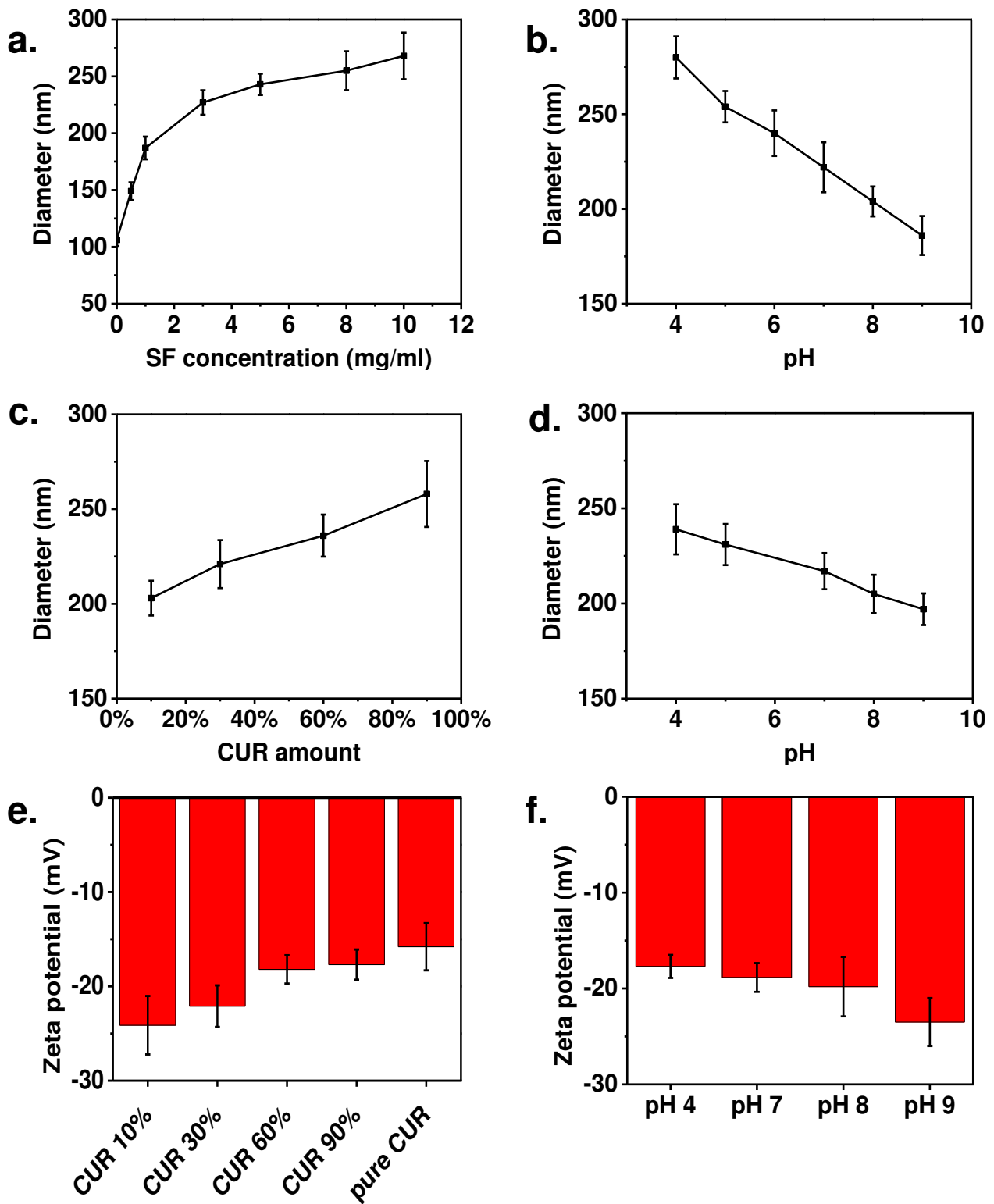


Fig.3. The effects of SF concentration, solution pH, and CUR amount to the particle size and zeta potential of MSPs and CMSPs. a) The effect of SF concentrations to the diameter of MSPs fabricated by sodium phosphate solutions (ionic strength: 1.25 M, pH 8). b) The effect of sodium phosphate solution pH to the diameter of MSPs (SF concentration: 5 mg/ml, sodium phosphate

ionic strength: 1.25M). c) & e) The effect of CUR amount to the diameter (c) and Zeta potential (e) of CMSPs, which were fabricated by adding different amounts of CUR (with weight equivalent to the percentages of SF used) to sodium phosphate solutions before SF solutions (5 mg/ml) and MNPs were added to the mixed solution. d) & f) The effect of sodium phosphate solution pH to the diameter (d) and Zeta potential (f) of CMSPs (SF concentration: 5 mg/ml, CUR amount: 10 % of SF used). The results are shown in mean \pm SD, $n \geq 4$. It was found that the size and Zeta potential of MSPs and CMSPs can be controlled by altering the SF concentration, solution pH and the amount of CUR used in the fabrication process.

To reveal the morphology of the particles before and after the CUR loading, AFM and TEM experiments have been carried out. AFM images of MSPs and CMSPs are shown in Fig.4a & b respectively. Spherical particles with a smooth surface were observed for MSPs, very similar to the morphology of the SFPs (Fig.1c). The diameter of the particles is around 250 nm, consistent with the data measured by DLS in Fig. 3a. In contrast, the surface of CMSPs appears to be rougher, indicating the loading of CUR into the particles. Presumably, the loading of CUR into the particles makes the particles more hydrophobic, therefore, the particles were dehydrated. Fig.4c & d showed the TEM images of MSPs and CMSPs respectively. These images indicate clearly that both MSPs and CMSPs are formed by multiple magnetic cores covered by SF or SF/ CUR shells, which is in agreement with the work by Tian *et al*⁴⁰. The insets in Fig.4c & d are the enlarged images from the red boxes. It can be seen from the enlarged images that the black magnetic cores are surrounded by SF shells. A number of smaller core-shell particles (~ 30 nm) aggregate to form a bigger particle (~ 250 nm).

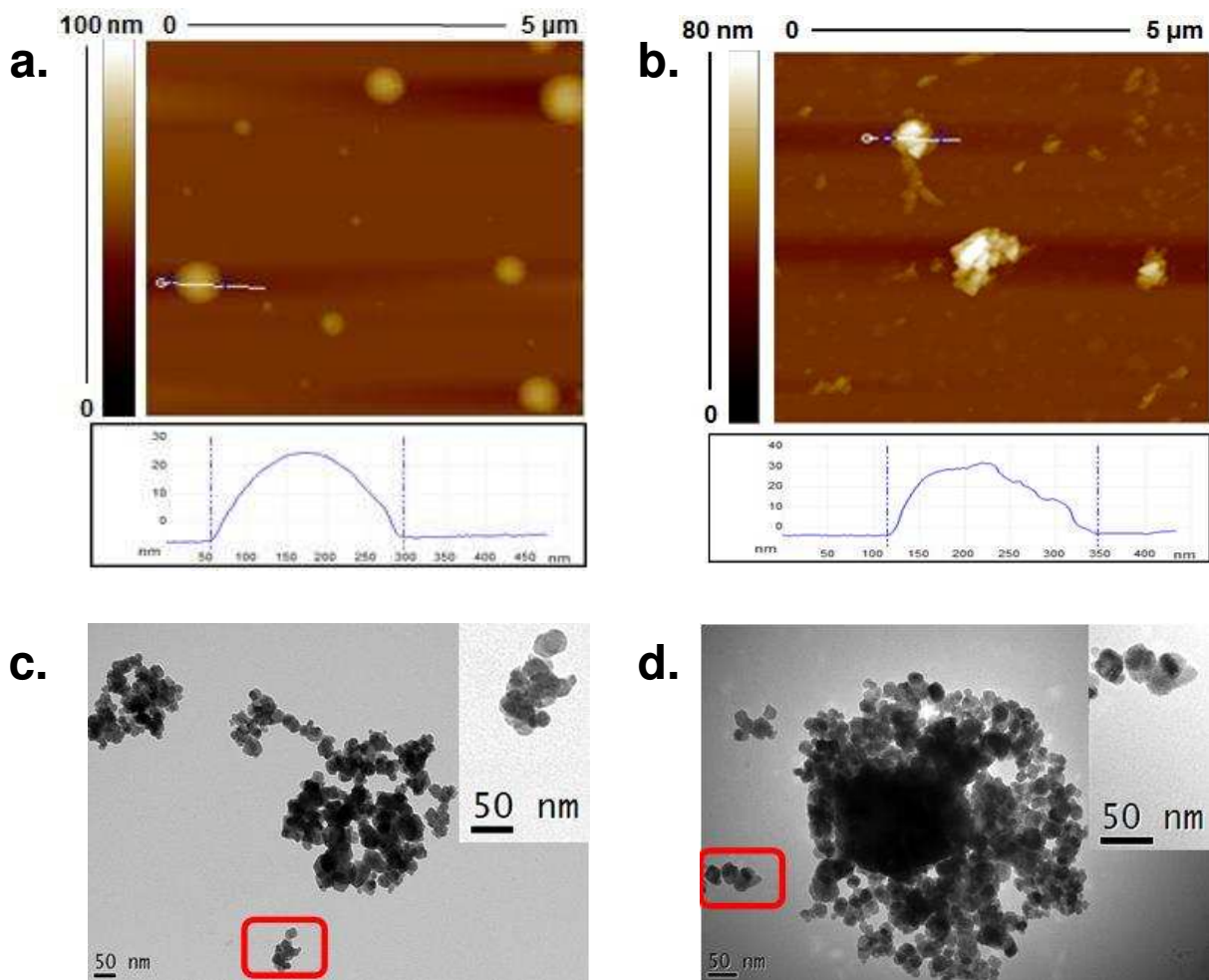


Fig.4. AFM and TEM images of the MSPs and CMSPs. a) & c) AFM and TEM images of MSPs (SF: 5 mg/ml, ionic strength of sodium phosphate: 1.25 M, pH 8). b) & d) AFM and TEM images of CMSPs (SF: 5 mg/ml, ionic strength of sodium phosphate: 1.25 M, pH 8, CUR amount: 10 % of SF used). Inserts are the enlarged images of from the red boxes.

3.3. Controlling loading and release of curcumin

To investigate the loading and release property of MSPs, diverse amounts of CUR were loaded into MSPs and the effect of sodium phosphate pH values was also investigated. Fig.5a illustrates the effect of CUR amount on encapsulation of CUR. The pH of sodium phosphate solution was fixed at 8 in this experiment. It can be seen that more than 97 % of CUR has been loaded into MSPs regardless of the amount of CUR used. Loading efficiency of CUR into these particles increased from ~ 10 % to ~ 80 % with the increasing amount of CUR used as shown in Fig.5c. The

encapsulation and loading efficiency of CUR in CMSPs is remarkably high given the fact that the typical loading efficiency for hydrophobic compound loading in protein nanoparticles is around 5%⁴⁷⁻⁵¹. To investigate the release profile of the CMSPs with different encapsulation and loading efficiencies, 5 mg of each type of particles were dispersed in 5 ml PBS (pH 7.4) and incubated at 37 °C with shaking (200 rpm, overnight). The CUR concentrations in solution were measured at different time scales and the cumulative CUR release curves are shown in Fig.5e. Although CMSPs with 10 % CUR loading released more in terms of percentage (12.4 % drug released in 20 days) of loaded CUR than others during the releasing period, the total amount of released CUR is still less than other (30%, 60% and 90% CUR loaded) particles. The drug release rate for CMSPs with 10 % CUR loading stays at a higher slope for the first 14 days and gradually level off, while for other particles, the release rates are still at steady slopes. The higher accumulative release rate was due to the low CUR loading⁵⁷.

Because the structure of SF particles can be controlled by using salt solution with different pH values, we have observed the loading / release profiles of CMSPs prepared at different pH values. Fig.5b & d illustrate the encapsulation and loading efficiencies of CUR in MSPs fabricated using sodium phosphate solutions with different pH values. It can be seen that MSPs fabricated by phosphate solutions with pH 4 - 8 have similar CUR encapsulation (over 97 %) and loading (over 10.5%) efficiencies, however, those using pH 9 solution showed noticeably less encapsulation (76 %) and loading (8.4 %) efficiencies than others. Fig.5f shows the cumulative CUR release of CMSPs fabricated using sodium phosphate with different pH values. CMSPs fabricated in pH 4 have released more CUR than those fabricated at higher pH values.

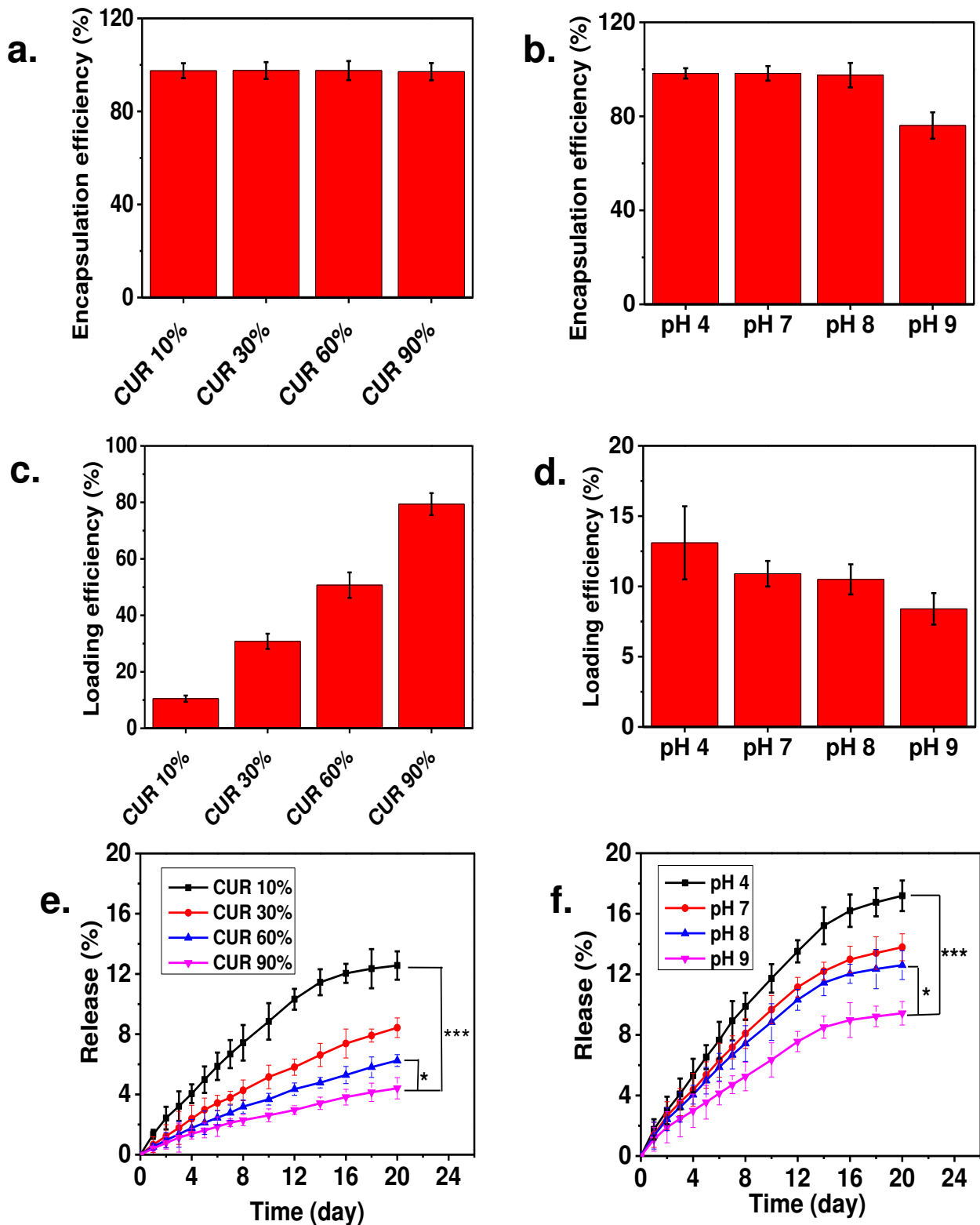


Fig.5. Drug leading and release profiles of the CMSPs. a) & b) Encapsulation efficiency of CMSPs fabricated with a) various CUR amounts in terms of the amount of SF used (pH 8) and b) various pH (CUR amount: 10 %). c) & d) Loading efficiency of CMSPs fabricated with c) various CUR usage

(pH 8) and d) various pH (CUR amount: 10 %). e) & f) Cumulative release of CUR from CMSPs fabricated with e) different CUR usage (pH 8) and f) different pH (CUR amount: 10 %). For each experiment, SF concentration was fixed at 5 mg/ml, ionic strength of sodium phosphate solution was fixed at 1.25 M. The results are shown in mean \pm SD, $n \geq 3$. The statistical significance is expressed as *** $p < 0.001$, ** $p < 0.01$, * $p < 0.05$.

3.4. *In vitro* cytotoxicity assay

MTT assay has been conducted to investigate the ability of CMSPs to inhibit growth of MDA-MB-231 cells. SFPs and MSPs were used as controls. SFPs, MSPs and CMSPs with 30 % CUR were incubated with MDA-MB-231 cells for 3 days before determining the relative cell viabilities. Free CURs with amount equal to that encapsulated by CMSPs were also incubated and the viabilities were compared with that from CMSPs. As illustrated in Fig.6, cell growth was significantly inhibited by either CMSPs or free CUR at higher CUR concentrations. Within the dose range from 3 to 100 $\mu\text{g/ml}$, CMSPs were significantly more cytotoxic to MDA-MB-231 cells than free CUR at equivalent CUR dosage. For instance, the cell viability of MDA-MB-231 cells treated with 60 $\mu\text{g/ml}$ CMSPs for 3 days was 12.2 ± 6.3 % and when treated with equivalent CUR, the viability was 46.3 ± 5.2 %, which suggests the inhibition of cancer cell growth was enhanced by CMSPs.

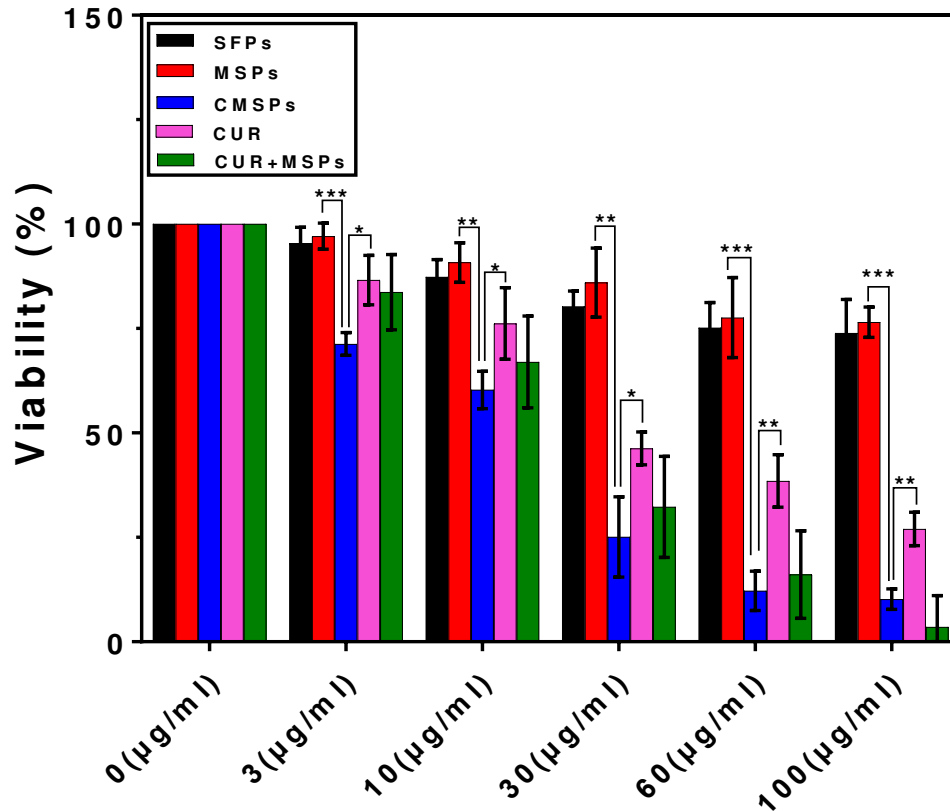


Fig.6. In vitro cytotoxicity studies for MDA-MB-231 cells treated with SFPs, MSPs, CMSPs (CUR usage: 30 %) and free CUR (amount equivalent to the CUR loaded in CMSPs) for 3 days. Added inhibitions of free CUR and MSPs equivalent to the amount of CUR and MSPs in CMSPs were also compared (CUR + MSPs). The results are shown in mean \pm SD, n = 8. The statistical significance is expressed as ***p < 0.001, **p < 0.01, *p < 0.05.

To investigate whether the higher cytotoxicity of CMSPs on MDA-MB-231 cells is a simple addition of CUR and MSPs cytotoxicity or enhanced CUR delivery by the nanoparticles, the growth inhibition result of CMSPs is compared with the added inhibition of corresponding free CUR and MSPs with amounts equal to the amounts of CUR and MSP content in CMSPs. The results shown in Fig.6 demonstrate that CMSPs have higher cytotoxicity than the added toxicities of free CUR and MSPs (except the data at 100 µg/ml). Therefore, the enhanced cytotoxicity of CMSPs against MDA-MB-231 cells is expected as a result of enhanced cell internalization of the CUR loaded particles.

3.5. Cellular uptake assays

To investigate the internalization and intracellular drug release behaviours of CMSPs, MDA-MB-231 cells were treated with different concentrations of CMSPs (with 30 % CUR loaded) and free CUR. The amount of free CUR was equal to the CUR content in CMSPs. The percentage of cell uptake of CUR is determined by flow cytometry and the results are shown in Fig.7a. The uptake efficiency of CUR for cells treated with CMSPs is significantly higher than those treated with free CUR at all concentrations and the difference is especially large at lower concentration. This result suggests that the enhanced growth inhibition effect of CMSPs, as illustrated in section 3.4, is a result from higher CMSPs uptake.

To investigate whether the uptake efficiency of CMSPs is significantly affected by the CUR content, MDA-MB-231 cells were incubated with SFPs, MSPs and CMSPs (30 % CUR loaded) for 24 h. The SF content of these particles was labelled with Rhodamine B which can be detected by flow cytometry to determine the uptake of these particles. These results are shown in Fig.7b. All three kind of particles displayed similar cellular uptake efficiency and uptake increased with the increasing particle concentration. Considerably high uptake efficiency (nearly 70 %) can be reached at lower concentration (e.g.10 $\mu\text{g/ml}$) which is beneficial to drug delivery.

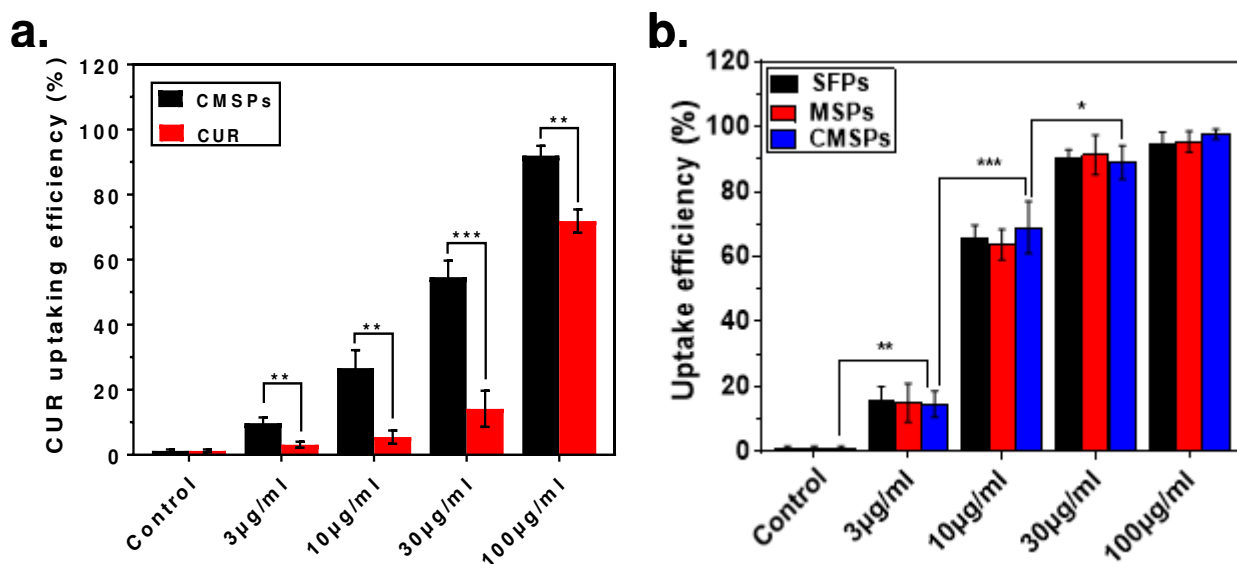


Fig.7. Cellular uptake assays of the different particles. a) CUR uptake in MDA-MB-231 cells after treated with CMSPs (with 30 % CUR loaded) and equivalent amount of free CUR for 24 h. b) Particle uptake efficiency of SFPs, MSPs and CMSPs in MDA-MB-231 cells after incubation for 24 h.

SF content in these particles was labelled with Rhodamine B and the uptake efficiencies were determined by measuring the cell population containing Rhodamine B fluorescence with flow cytometry. The results are shown in mean \pm SD, n = 3. The statistical significance is expressed as ***p < 0.001, **p < 0.01, *p < 0.05. It was found that cells treated with CMSPs had significantly higher uptake efficiency of CUR than those treated with free CUR.

Fig.8 shows the fluorescent microscopic images of CUR uptake by MDA-MB-231 cells after incubation with free CUR (Fig.8a & b) or CMSPs (Fig.8c & d). CUR molecule is auto-fluorescent (Ex 340 nm, Em 530 nm⁴¹) and was observed with GFP channel. The nucleus and cytoskeleton were stained with DAPI and Texas Red®-X Phalloidin. The enhanced CUR uptake effect of CMSPs is confirmed by these images. As shown in Fig.8a & b, the green fluorescence in cells that have been treated the free CUR, is very weak which suggests the uptake efficiency of free CUR is low, consistent with uptake efficiency shown in Fig.7a. In contrast, Fig.8c & d shows that over 90 % of the cells incubated with CMSPs have displayed much brighter green fluorescence which appears to be quite uniformly distributed within the cytosol. The dramatically increased fluorescence intensity suggests that CMSPs can significantly enhance the uptake of CUR for MDA-MB-231 cells. The yellow fluorescence in the merged images indicates the co-localization of the Texas red and CUR fluorescence.

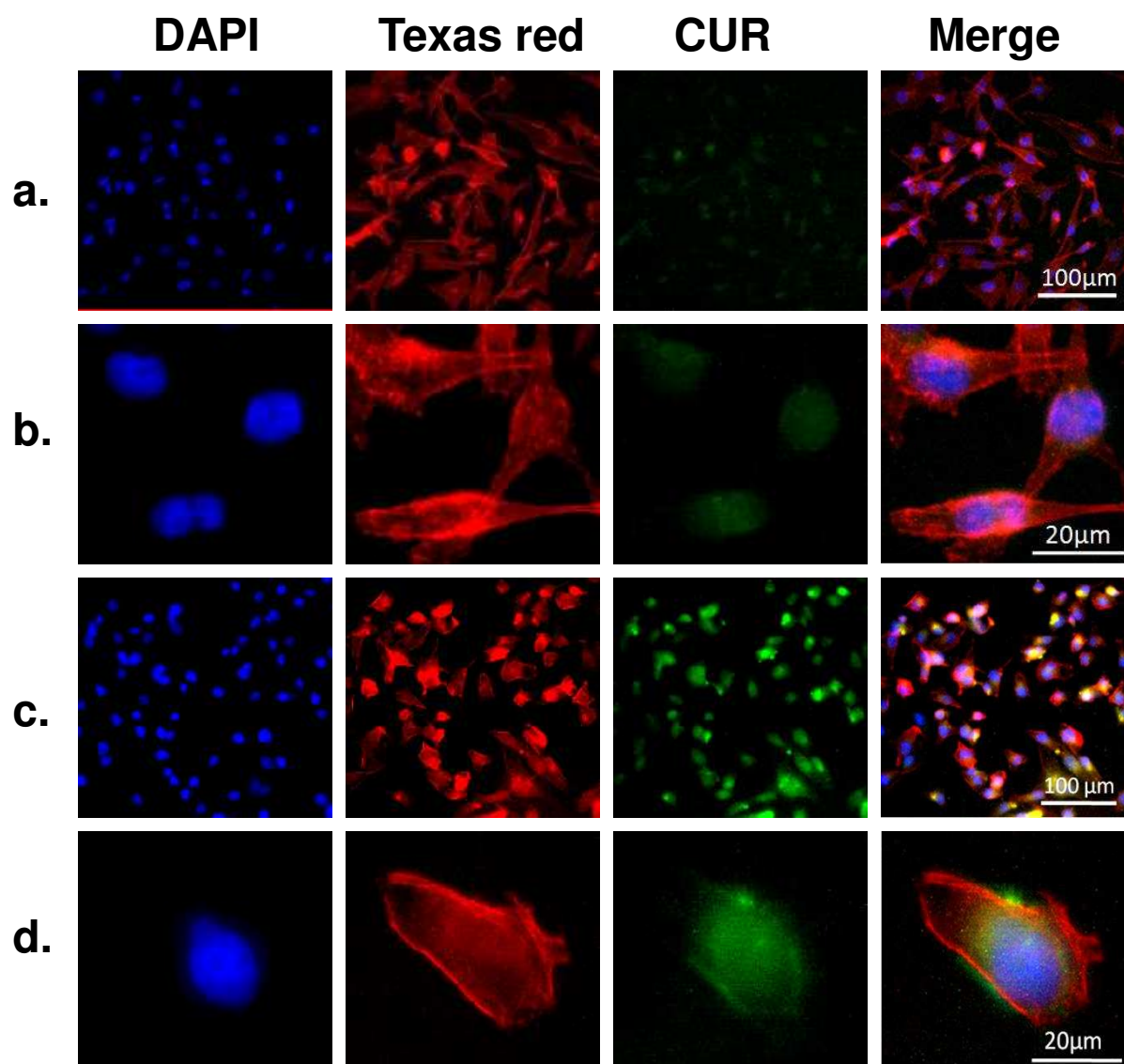


Fig.8. Representative microscopic images of MDA-MB-231 cells incubated with free CUR (a & b, CUR amount (10 µg/ml) equivalent to the CUR loaded in CMSPs (30%)) and CMSPs (c & d, 30 µg/ml) for 4 h. Cell nucleus and cytoskeleton were stained with DAPI (blue) and Texas red (red); all images were taken with AF6000 microscope (Leica). Comparing the images in a & b to c & d, it can be seen that CMSPs significantly improve the cellular uptake of the CUR.

To demonstrate the uptake of the nanoparticles, Fig.9 shows the fluorescent microscopic images of FITC-labelled SFPs (Fig.9a & b) and MSPs (Fig.9c & d) uptake by MDA-MB-231 cells. It can be seen from Fig.9a & c that over 90 % of the cells have green fluorescence, consistent with uptake efficiency shown in Fig.7b. Fig.9b & d shows the uptake by single cells.

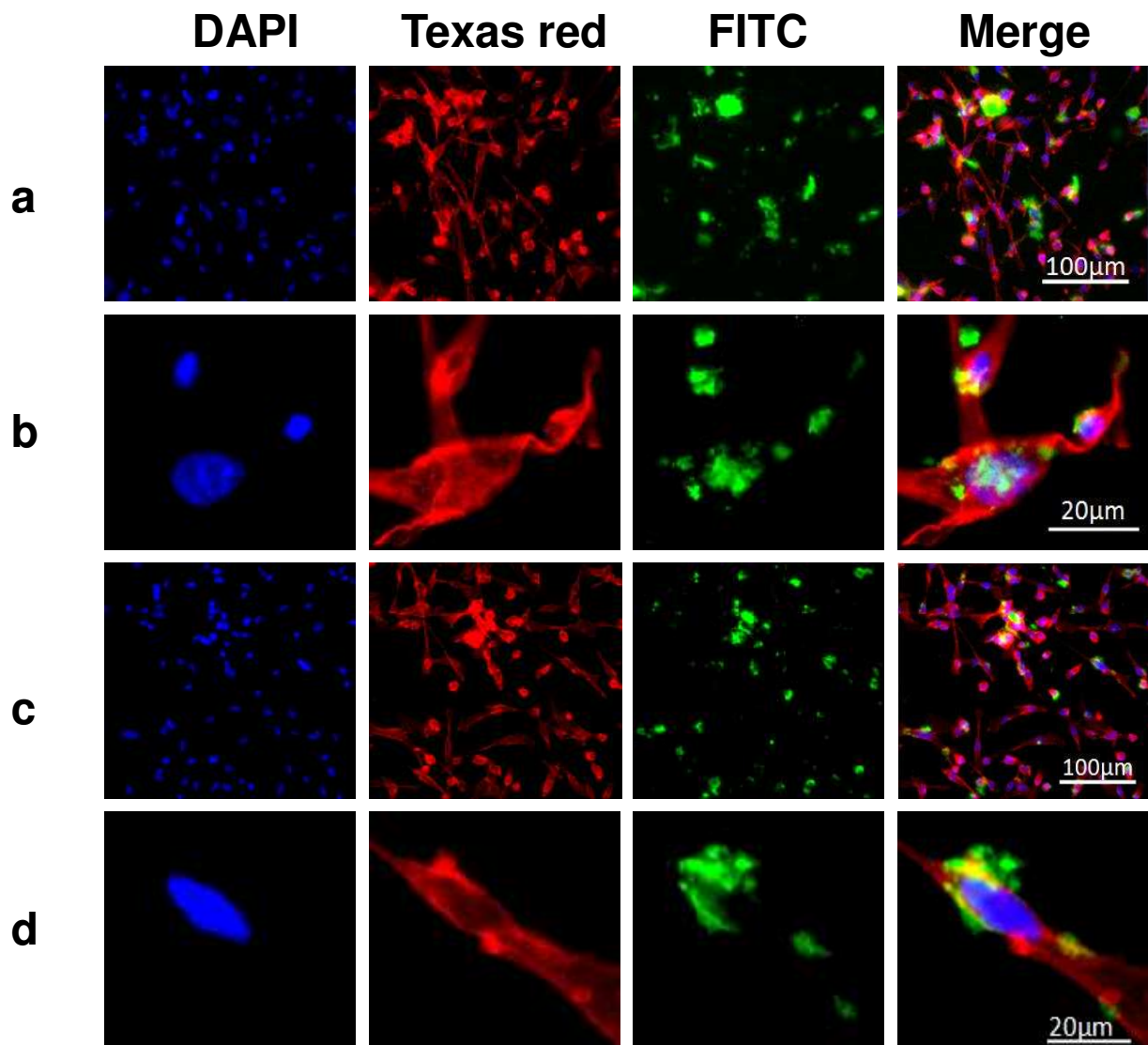


Fig.9. Representative microscopic images of MDA-MB-231 cells incubated with FITC-labelled SFPs (a & b, 30 µg/ml) or FITC labelled MSPs (c & d, 30 µg/ml). Cell nucleus and cytoskeleton were stained with DAPI (blue) and Texas red (red); all images were taken with AF6000 microscope (Leica).

4. Discussion

Desolvation and salting-out are two common methods for the fabrication of SF particles⁴³. While the desolvation method⁴⁴ is capable of making relatively smaller SFPs (< 200 nm), toxic organic solvents such as ethanol, methanol or acetone have to be introduced in the process, which may increase the toxicity to cells. On the other hand, SF particles can be prepared by the salting-out method without organic solvents involved. Therefore, we have chosen the salting-out method for

the fabrication of SFPs in our experiment. In the process of salting-out, SF protein chains will first form micellar-like structures in a salt solution due to the enhancement of hydrophobic interactions. The particulate globules will then be formed with the micelles by further hydrophobic interactions³⁷. With the salting-out method reported by Kaplan and co-workers, only larger SFPs (0.62 - 2.12 μm) can be produced. However, the sizes of the particles are bigger than the desired size for drug delivery. For example, it has been reported that nanoparticles in the range of 100 - 200 nm can extravasate through vascular fenestrations of tumours and escape filtration by liver and spleen³⁸. Nanoparticles with diameter ~ 100 nm are long-lasting in circulation, as the size increased to 150 nm and larger, more and more nanoparticles become entrapped in the liver and spleen³⁸. Therefore, it is likely that lots of these SF nanoparticles SFPs with diameters over 600 nm will be filtered by the liver and spleen instead of reaching the tumour site once injected into human body. In contrast, those fabricated with sodium phosphate showed much smaller sizes (90 - 300 nm) and narrower size distributions (Fig.1a). Therefore, it provides a method to prepare SFPs with more appropriate sizes for drug delivery without involving organic solvent. The explanation for the difference in nanoparticle size created using sodium phosphate and potassium phosphate is to be found in the difference in size of the cations (Hofmeister effect). Sodium is relatively small and has a higher charge density than the larger potassium ion. The cations will be interacting directly but weakly with the partial charges on the neutral SF. The cations strongest effect is likely to be indirect through the cations interactions with water or through the interaction of the cation with the phosphate anion. For a self-assembly reaction involving multiple intermolecular beta-pleated sheet interactions involved in SFP formation there will be an initial dimerization with a high activation energy followed by multiple subsequent additions of fibroin monomers with a lower activation energy. The presence of the higher charge density cation has reduced the activation energy of the initial dimer formation resulting in greater nucleation and numerous small SFPs. Why this happens is subject to conjecture. Phosphate is known to indirectly drive protein self-association through competition for water⁴⁵ and a phenomenological theory is that low charge density ions like potassium negate the effect of the high charge density phosphate⁴⁶, in this case resulting in fewer larger SFPs.

The results also showed that the diameter of SFPs, MSPs and CMSPs decrease with the increase of sodium phosphate pH value which suggests that the property of MSPs and CMSPs is dominated by their SF content. It can be assumed that when the MSPs or CMSPs were prepared in a pH 9

solution, the SF coating became more negatively charged and less hydrophobic, which tend to increase the repulsion and decrease the hydrophobic interaction among MSPs or CMSPs and eventually fabricate smaller particles. Therefore, the size of MSPs or CMSPs can be controlled by altering the pH value of salt solution used in the process.

Our results revealed that remarkably high encapsulation (>97 %) and loading (10% - 80%) efficiency of CUR can be achieved in the CMSPs fabrication process, while typical loading efficiency for hydrophobic compound loading in protein nanoparticles is around 5%⁴⁷⁻⁵¹. This phenomenon could owe to the strong hydrophobic interaction between hydrophobic CUR and the water-insoluble silk-II structure formed during the salting-out process. Our results have shown significant improvement in loading efficiency (up to 80%) compared with 6% found for CUR-loading into SF/poly(L-lactic acid-co-ε-caprolactone) (P(LLA-CL)) nanofibrous scaffolds⁵², 12% for the silk/CUR nanoparticles fabricated in supercritical CO₂⁵³, 15% for the SFPs reported by Li *et al.*⁵⁴, 30% for the silk/CUR nanoparticles produced by desolvation method⁵⁵, as well as 10% loading efficiency for the paclitaxel loaded SFPs⁵⁶. The lower loading efficiency in SFPs via desolvation method was due to the fact that CUR tend to dissolve in organic solvent instead of adsorb on SF nanoparticles SFPs. However, for loading via salting-out method, the hydrophobic CUR was either encapsulated in or adsorbed on the water-insoluble SFPs instead of suspend in the aqueous solution. Therefore, the loading of CUR in SFPs via salting-out method is more suitable for the fabrication of high CUR-loading SFPs, which is desired for the drug delivery systems.

Another desired capability of a drug carrier is to be able to control the release of drug and normally a longer releasing period is desired. It should be noted that our release profile last 20 days with up to 12% release of the CUR which is significant better than the literature which normally last only one week⁵³⁻⁵⁵. During the whole period of CUR releasing, the release was progressive without obvious burst release, which indicates that the CUR was homogeneously dispersed in the CMSPs. This release profile was also in agreement with the work by Xie *et al.*⁵³ that the inconspicuous burst release was due to the poor water-solubility of CUR. The release profile of CUR from SF matrix can be described as a three-step process; firstly, the initial diffusion resulted from desorption of CUR from the particle surface, then water penetrates into the matrix and the inner drugs are released. Finally, the degradation of SF releases the remaining encapsulated drug⁵⁸. Since the burst release

of CUR is limited by its poor solubility, the CUR release can be assumed that depend on the solubility, diffusion and biodegradation of the SF matrix. It has been reported that the change of SF structure can lead to a different release profile of CUR⁵⁹. Xie *et al.*⁵³ found that silk I structure of SF nanofibrous become more water-insoluble when exposed to ethanol vapour, and the ethanol vapour treated SF carriers showed a lower CUR release rate than the no-treated ones. Li *et al.*⁵⁴ have prepared CUR loaded SFPs by desolvation method, the resulted SF carriers have released only ~ 5 % of loaded CUR and nearly stopped releasing after 3 days. This low CUR release amount and short release period can be explained by the fact that water-insoluble β -sheet structures were formed after the SF have been treated with ethanol⁴⁴, thus the hydrophobic CUR tend to remain in hydrophobic SF matrix,

It has been observed that the loading / release profiles of CMSPs can be controlled by the pH value of salt solution used. For instance CMSPs fabricated using pH 9 salt solution showed noticeably less encapsulation and loading efficiency and also released fewer CUR. On the other hand, CMSPs fabricated using pH 4 salt solution have released more CUR than those fabricated at higher pH values. Considering the results shown in Fig.1f that MSPs fabricated with pH 9 sodium phosphate solutions have more silk-I content than those fabricated in lower pH values, we suspect that the secondary structure of SF significantly affects the ability of MSPs in absorbing CUR and the less hydrophobic silk-I content is less capable of capturing CUR. For CMSPs fabricated at pH 4, the CUR loading was carried out at pH 4 while SF was more hydrophobic and the release was carried out at pH 7.4, at which pH the SF become less hydrophobic therefore facilitate the release of the hydrophobic CUR. Therefore, the release of CUR depends on the charge and structure of SF which can be controlled during the salting-out process. These results suggest that CMSPs possess many desired properties such as high encapsulation / loading efficiency and controllable release profile, which makes it a promising system for drug delivery. The results also revealed that the inhibition of cancer cell growth by CUR was enhanced by CMSPs.

The enhanced toxicity of CMSPs could be the result of enhanced uptake of CMSPs by cells and the encapsulated CUR was released via diffusion or the degradation⁵³ of SF matrix inside the cells, which in turn increased the up take efficiency of CUR, thus decreased the cell viability. SFPs and MSPs, on the other hand, had very little effect on cell toxicity at lower concentration and relatively

low cytotoxicity at higher concentrations, indicating that SF nanoparticles SFPs and MSP are non-toxic nanoparticles. Similar studies have been reported and indicated that SF particles also showed no cytotoxicity to many other cell lines^{31, 40, 56, 59}. For example, Xie *et al.*⁵⁹ have compared the in vitro anti-cancer effect of CUR and CUR loaded SF nanoparticles SFPs against HCT-116 cancer cells. It was found that the CUR-SF nanofibrous matrix had equivalent anti-cancer effect to the DMSO dissolved CUR.

The enhanced cellular uptake of CUR by CMSPs has also been observed in the results, Since CUR is a highly hydrophobic drug, its dispersion and diffusion in aqueous solution is significantly poor. However, when loaded in CMSPs, CUR was encapsulated within CMSPs and can cross the cell membrane for cell uptake. The results are consistent with the reports that SF particles can be taken up rapidly by cells³¹⁻³².

Conclusions

Smaller particles as drug carriers are desired for drug delivery systems. However, SF particles fabricated using potassium phosphate are relatively larger (500 -1200 nm). In this paper, we developed a method to fabricate SFPs using sodium phosphate and the results indicated that SFPs fabricated with sodium phosphate possess significantly smaller size compared with those fabricated using potassium phosphate. This new method provides a simple process allowing us to fabricate smaller SFPs without using any solvent. Size and secondary structure of SFPs can be controlled by changing SF concentration, the pH and ionic strength of sodium phosphate solutions. The size, zeta potential and drug loading/releasing efficiency of CMSPs can be controlled by using different SF concentrations, CUR amounts and pH values of sodium phosphate solutions. Sustained release of CUR from CMSPs was observed for 20 days and CMSPs fabricated at lower pH values showed higher CUR release rate. Enhanced growth inhibition of CMSPs against MDA-MB-231 cells was observed in MTT assay and CUR uptake efficiency was also significantly enhanced due to the better internalization of CMSPs. The effect of particle concentration on cellular uptake efficiency was investigated and the results indicate that uptake efficiency can be increased by increasing particle concentration. In addition, these particles displayed similar uptake efficiency, which suggests the CUR content in CMSPs did not affect the uptake efficiency of particles. Therefore,

CMSPs can be used as potential drug delivery system for cancer therapy.

Acknowledgements

The authors would like to thank EPSRC (EP/N023579/1), Royal Society (RG160662) and University of Sheffield for support.

References:

1. Chattopadhyay, I.; Biswas, K.; Bandyopadhyay, U.; Banerjee, R. K., Turmeric and curcumin: Biological actions and medicinal applications. *Curr. Sci.(Bangalore)* **2004**, *87* (1), 44-53
2. Ammon, H. P.; Wahl, M. A., Pharmacology of *Curcuma longa*. *Planta Med.* **1991**, *57* (01), 1-7,doi:10.1055/s-2006-960004.
3. Masuda, T.; Hidaka, K.; Shinohara, A.; Maekawa, T.; Takeda, Y.; Yamaguchi, H., Chemical studies on antioxidant mechanism of curcuminoid: analysis of radical reaction products from curcumin and Linoleate. *J. Agric. Food Chem.* **1999**, *47* (1), 71-77,doi: 10.1021/jf9805348.
4. Ruby, A.; Kuttan, G.; Babu, K. D.; Rajasekharan, K.; Kuttan, R., Anti-tumour and antioxidant activity of natural curcuminoids. *Cancer Lett.* **1995**, *94* (1), 79-83,doi:10.1016/0304-3835(95)03827-J.
5. Ak, T.; Gulcin, I., Antioxidant and radical scavenging properties of curcumin. *Chem Biol Interact* **2008**, *174* (1), 27-37,doi:10.1016/j.cbi.2008.05.003.
6. Brouet, I.; Ohshima, H., Curcumin, an anti-tumor promoter and anti-inflammatory agent, inhibits induction of nitric oxide synthase in activated macrophages. *Biochem. Biophys. Res. Commun.* **1995**, *206* (2), 533-540,doi:10.1006/bbrc.1995.1076.
7. Kawamori, T.; Lubet, R.; Steele, V. E.; Kelloff, G. J.; Kaskey, R. B.; Rao, C. V.; Reddy, B. S., Chemopreventive effect of curcumin, a naturally occurring anti-inflammatory agent, during the promotion/progression stages of colon cancer. *Cancer Res.* **1999**, *59* (3), 597-601
8. Aggarwal, B. B.; Harikumar, K. B., Potential therapeutic effects of curcumin, the anti-inflammatory agent, against neurodegenerative, cardiovascular, pulmonary, metabolic, autoimmune and neoplastic diseases. *Int J Biochem Cell Biol* **2009**, *41* (1), 40-59,doi:10.1016/j.biocel.2008.06.010.
9. Sidhu, G. S.; Singh, A. K.; Thaloor, D.; Banaudha, K. K.; Patnaik, G. K.; Srimal, R. C.; Maheshwari, R. K., Enhancement of wound healing by curcumin in animals. *Wound Repair Regen.* **1998**, *6* (2), 167-177,doi:10.1046/j.1524-475X.1998.60211.x.
10. Panchatcharam, M.; Miriyala, S.; Gayathri, V. S.; Suguna, L., Curcumin improves wound healing by modulating collagen and decreasing reactive oxygen species. *Mol Cell Biochem* **2006**, *290* (1), 87-96,doi:10.1007/s11010-006-9170-2.
11. Negi, P.; Jayaprakasha, G.; Jagan Mohan Rao, L.; Sakariah, K., Antibacterial activity of turmeric oil: a byproduct from curcumin manufacture. *J. Agric. Food Chem.* **1999**, *47* (10), 4297-4300,doi:10.1021/jf990308d.
12. Mun, S. H.; Joung, D. K.; Kim, Y. S.; Kang, O. H.; Kim, S. B.; Seo, Y. S.; Kim, Y. C.; Lee, D. S.; Shin, D. W.; Kweon, K. T.; Kwon, D. Y., Synergistic antibacterial effect of curcumin against methicillin-resistant *Staphylococcus aureus*. *Phytomedicine* **2013**, *20* (8), 714-718,doi:10.1016/j.phymed.2013.02.006.
13. Rezaee, R.; Momtazi, A. A.; Monemi, A.; Sahebkar, A., Curcumin: a potentially powerful tool to reverse cisplatin-induced toxicity. *Pharmacol. Res* **2016**, *117*, 218-227,doi: 10.1016/j.phrs.2016.12.037.
14. Ganjali, S.; Blesso, C. N.; Banach, M.; Pirro, M.; Majeed, M.; Sahebkar, A., Effects of curcumin on HDL functionality. *Pharmacol. Res* **2017**, *119*, 208-218,doi:10.1016/j.phrs.2017.02.008.

15. Wilken, R.; Veena, M. S.; Wang, M. B.; Srivatsan, E. S., Curcumin: A review of anti-cancer properties and therapeutic activity in head and neck squamous cell carcinoma. *Mol Cancer* **2011**, *10* (1), 12,doi:10.1186/1476-4598-10-12.
16. Aggarwal, B. B.; Kumar, A.; Bharti, A. C., Anticancer potential of curcumin: preclinical and clinical studies. *Anticancer res* **2003**, *23* (1A), 363-398
17. Li, M.; Zhang, Z.; Hill, D. L.; Wang, H.; Zhang, R., Curcumin, a dietary component, has anticancer, chemosensitization, and radiosensitization effects by down-regulating the MDM2 oncogene through the PI3K/mTOR/ETS2 pathway. *Cancer Res* **2007**, *67* (5), 1988-1996,doi:10.1158/0008-5472.CAN-06-3066.
18. Tapal, A.; Tiku, P. K., Complexation of curcumin with soy protein isolate and its implications on solubility and stability of curcumin. *Food Chem.* **2012**, *130* (4), 960-965,doi:10.1016/j.foodchem.2011.08.025.
19. Wan, S.; Sun, Y.; Qi, X.; Tan, F., Improved bioavailability of poorly water-soluble drug curcumin in cellulose acetate solid dispersion. *AAPS PharmSciTech* **2012**, *13* (1), 159-166,doi:10.1208/s12249-011-9732-9.
20. Bisht, S.; Maitra, A., Systemic delivery of curcumin: 21st century solutions for an ancient conundrum. *Curr. Drug Discovery Technol.* **2009**, *6* (3), 192-199,doi:10.2174/157016309789054933.
21. Anand, P.; Kunnumakkara, A. B.; Newman, R. A.; Aggarwal, B. B., Bioavailability of curcumin: problems and promises. *Mol Pharm* **2007**, *4* (6), 807-818,doi:10.1021/mp700113r.
22. Rahimi, H. R.; Nedaeinia, R.; Shamloo, A. S.; Nikdoust, S.; Oskuee, R. K., Novel delivery system for natural products: Nano-curcumin formulations. *AJP* **2016**, *6* (4), 383-398
23. Shehzad, A.; Khan, S.; Shehzad, O.; Lee, Y. S., Curcumin therapeutic promises and bioavailability in colorectal cancer. *Drugs Today (Barc)* **2010**, *46* (7), 523-532,doi:10.1358/dot.2010.46.7.1509560.
24. Li, L.; Braiteh, F. S.; Kurzrock, R., Liposome-encapsulated curcumin: in vitro and in vivo effects on proliferation, apoptosis, signaling, and angiogenesis. *J. Clin. Oncol.* **2005**, *104* (6), 1322-1331,doi:10.1002/cncr.21300.
25. Liu, A.; Lou, H.; Zhao, L.; Fan, P., Validated LC/MS/MS assay for curcumin and tetrahydrocurcumin in rat plasma and application to pharmacokinetic study of phospholipid complex of curcumin. *J Pharm Biomed Anal* **2006**, *40* (3), 720-727,doi:10.1016/j.jpba.2005.09.032.
26. Cruz-Correa, M.; Shoskes, D. A.; Sanchez, P.; Zhao, R.; Hyland, L. M.; Wexner, S. D.; Giardiello, F. M., Combination treatment with curcumin and quercetin of adenomas in familial adenomatous polyposis. *Clin Gastroenterol Hepatol* **2006**, *4* (8), 1035-1038,doi:10.1016/j.cgh.2006.03.020.
27. Tiyaaboonchai, W.; Tungpradit, W.; Plianbangchang, P., Formulation and characterization of curcuminoids loaded solid lipid nanoparticles. *Int J Pharm* **2007**, *337* (1), 299-306,doi:10.1016/j.ijpharm.2006.12.043.
28. Vepari, C.; Kaplan, D. L., Silk as a Biomaterial. *Prog Polym Sci* **2007**, *32* (8), 991-1007,doi:10.1016/j.progpolymsci.2007.05.013.
29. Dal Pra, I.; Freddi, G.; Minic, J.; Chiarini, A.; Armato, U., De novo engineering of reticular connective tissue in vivo by silk fibroin nonwoven materials. *Biomaterials* **2005**, *26* (14), 1987-1999,doi:10.1016/j.biomaterials.2004.06.036.
30. Horan, R. L.; Antle, K.; Collette, A. L.; Wang, Y.; Huang, J.; Moreau, J. E.; Volloch, V.; Kaplan, D. L.; Altman, G. H., In vitro degradation of silk fibroin. *Biomaterials* **2005**, *26* (17), 3385-3393,doi:10.1016/j.biomaterials.2004.09.020.
31. Gupta, V.; Aseh, A.; Rios, C. N.; Aggarwal, B. B.; Mathur, A. B., Fabrication and characterization of silk fibroin-derived curcumin nanoparticles for cancer therapy. *Int J Nanomedicine* **2009**, *4* (1), 115-122,doi:10.2147/IJN.S5581.
32. Kundu, J.; Chung, Y. I.; Kim, Y. H.; Tae, G.; Kundu, S. C., Silk fibroin nanoparticles for cellular uptake and control release. *Int J Pharm* **2010**, *388* (1), 242-250,doi:10.1016/j.ijpharm.2009.12.052.
33. Bessa, P. C.; Balmayor, E. R.; Azevedo, H. S.; Nurnberger, S.; Casal, M.; van Griensven, M.; Reis, R. L.; Redl, H., Silk fibroin microparticles as carriers for delivery of human recombinant BMPs. Physical characterization and drug release. *J Tissue Eng Regen Med* **2010**, *4* (5), 349-355,doi:10.1002/term.245.
34. Shi, P.; Goh, J. C., Release and cellular acceptance of multiple drugs loaded silk fibroin particles. *Int J Pharm* **2011**,

420 (2), 282-289,doi:10.1016/j.ijpharm.2011.08.051.

35. Chen, M.; Shao, Z.; Chen, X., Paclitaxel-loaded silk fibroin nanospheres. *J Biomed Mater Res A* **2012**, *100* (1), 203-210,doi:10.1002/jbm.a.33265.
36. Zhao, Z.; Li, Y.; Chen, A.-Z.; Zheng, Z.-J.; Hu, J.-Y.; Li, J.-S.; Li, G., Generation of Silk Fibroin Nanoparticles via Solution-Enhanced Dispersion by Supercritical CO₂. *Ind. Eng. Chem. Res.* **2013**, *52* (10), 3752-3761,doi:10.1021/ie301907f.
37. Lammel, A. S.; Hu, X.; Park, S. H.; Kaplan, D. L.; Scheibel, T. R., Controlling silk fibroin particle features for drug delivery. *Biomaterials* **2010**, *31* (16), 4583-4591,doi:10.1016/j.biomaterials.2010.02.024.
38. Blanco, E.; Shen, H.; Ferrari, M., Principles of nanoparticle design for overcoming biological barriers to drug delivery. *Nat Biotechnol* **2015**, *33* (9), 941-951,doi:10.1038/nbt.3330.
39. Arruebo, M.; Fernández-Pacheco, R.; Ibarra, M. R.; Santamaría, J., Magnetic nanoparticles for drug delivery. *Nano today* **2007**, *2* (3), 22-32,doi:10.1016/S1748-0132(07)70084-1.
40. Tian, Y.; Jiang, X.; Chen, X.; Shao, Z.; Yang, W., Doxorubicin-loaded magnetic silk fibroin nanoparticles for targeted therapy of multidrug-resistant cancer. *Adv Mater* **2014**, *26* (43), 7393-7398,doi:10.1002/adma.201403562.
41. Crivello, J. V.; Bulut, U., Curcumin: A naturally occurring long-wavelength photosensitizer for diaryliodonium salts. *Poly.Chem.* **2005**, *43* (21), 5217-5231,doi:10.1002/pola.21017.
42. Hu, X.; Kaplan, D.; Cebe, P., Determining Beta-Sheet Crystallinity in Fibrous Proteins by Thermal Analysis and Infrared Spectroscopy. *Macromolecules* **2006**, *39* (18), 6161-6170,doi:10.1021/ma0610109.
43. Zhao, Z.; Li, Y.; Xie, M. B., Silk fibroin-based nanoparticles for drug delivery. *Int J Mol Sci* **2015**, *16* (3), 4880-4903,doi:10.3390/ijms16034880.
44. Zhang, Y.-Q.; Shen, W.-D.; Xiang, R.-L.; Zhuge, L.-J.; Gao, W.-J.; Wang, W.-B., Formation of silk fibroin nanoparticles in water-miscible organic solvent and their characterization. *J. Nanopart. Res.* **2006**, *9* (5), 885-900,doi:10.1007/s11051-006-9162-x.
45. Bye, J. W.; Falconer, R. J., Three stages of lysozyme thermal stabilization by high and medium charge density anions. *J. Phys. Chem. B* **2014**, *118* (16), 4282-4286,doi:10.1021/jp412140v.
46. Collins, K. D., Charge density-dependent strength of hydration and biological structure. *Biophys. J.* **1997**, *72* (1), 65-76,doi:10.1016/S0006-3495(97)78647-8.
47. Patel, A.; Hu, Y.; Tiwari, J. K.; Velikov, K. P., Synthesis and characterisation of zein-curcumin colloidal particles. *Soft Matter* **2010**, *6* (24), 6192-6199,doi:10.1039/C0SM00800A.
48. Hu, D.; Lin, C.; Liu, L.; Li, S.; Zhao, Y., Preparation, characterization, and in vitro release investigation of lutein/zein nanoparticles via solution enhanced dispersion by supercritical fluids. *J. Food Eng.* **2012**, *109* (3), 545-552,doi:10.1016/j.jfoodeng.2011.10.025.
49. Luo, Y.; Teng, Z.; Wang, Q., Development of zein nanoparticles coated with carboxymethyl chitosan for encapsulation and controlled release of vitamin D3. *J. Agric. Food Chem.* **2012**, *60* (3), 836-843,doi:10.1021/jf204194z.
50. Chen, J.; Zheng, J.; McClements, D. J.; Xiao, H., Tangeretin-loaded protein nanoparticles fabricated from zein/ β -lactoglobulin: Preparation, characterization, and functional performance. *Food Chem.* **2014**, *158*, 466-472,doi:10.1016/j.foodchem.2014.03.003.
51. Maghsoudi, A.; Shojaosadati, S. A.; Farahani, E. V., 5-Fluorouracil-loaded BSA nanoparticles: formulation optimization and in vitro release study. *AAPS PharmSciTech* **2008**, *9* (4), 1092-1096,doi:10.1208/s12249-008-9146-5.
52. Lian, Y.; Zhan, J.-C.; Zhang, K.-H.; Mo, X.-M., Fabrication and characterization of curcumin-loaded silk fibroin/P (LLA-CL) nanofibrous scaffold. *Front Mater Sci* **2014**, *8* (4), 354-362,doi:10.1007/s11706-014-0270-8.
53. Xie, M.-B.; Li, Y.; Zhao, Z.; Chen, A.-Z.; Li, J.-S.; Hu, J.-Y.; Li, G.; Li, Z., Solubility enhancement of curcumin via supercritical CO₂ based silk fibroin carrier. *J. Supercrit. Fluids* **2015**, *103*, 1-9,doi:10.1016/j.supflu.2015.04.021.
54. Li, H.; Tian, J.; Wu, A.; Wang, J.; Ge, C.; Sun, Z., Self-assembled silk fibroin nanoparticles loaded with binary drugs in the treatment of breast carcinoma. *Int. J. Nanomed.* **2016**, *11*, 4373-4380,doi:10.2147/IJN.S108633.

55. Perteghella, S.; Crivelli, B.; Catenacci, L.; Sorrenti, M.; Bruni, G.; Necchi, V.; Vigani, B.; Sorlini, M.; Torre, M. L.; Chlapanidas, T., Stem cell-extracellular vesicles as drug delivery systems: New frontiers for silk/curcumin nanoparticles. *Int. J. Pharm.* **2017**, *520* (1), 86-97,doi: 10.1016/j.ijpharm.2017.02.005.
56. Wu, P.; Liu, Q.; Li, R.; Wang, J.; Zhen, X.; Yue, G.; Wang, H.; Cui, F.; Wu, F.; Yang, M., Facile preparation of paclitaxel loaded silk fibroin nanoparticles for enhanced antitumor efficacy by locoregional drug delivery. *ACS Appl. Mater. Interfaces* **2013**, *5* (23), 12638-12645,doi:10.1021/am403992b@proofing.
57. Kumari, A.; Yadav, S. K.; Yadav, S. C., Biodegradable polymeric nanoparticles based drug delivery systems. *Colloids Surf., B* **2010**, *75* (1), 1-18,doi:10.1016/j.colsurfb.2009.09.001.
58. Huang, X.; Brazel, C. S., On the importance and mechanisms of burst release in matrix-controlled drug delivery systems. *J. Controlled Release* **2001**, *73* (2), 121-136,doi:10.1016/S0168-3659(01)00248-6.
59. Xie, M.; Fan, D.; Chen, Y.; Zhao, Z.; He, X.; Li, G.; Chen, A.; Wu, X.; Li, J.; Li, Z., An implantable and controlled drug-release silk fibroin nanofibrous matrix to advance the treatment of solid tumour cancers. *Biomaterials* **2016**, *103*, 33-43,doi:10.1016/j.biomaterials.2016.06.049.

For Table of Contents Use Only

Magnetic-Silk Core-Shell Nanoparticles as Potential Carriers for Targeted Delivery of Curcumin into Human Breast Cancer Cells

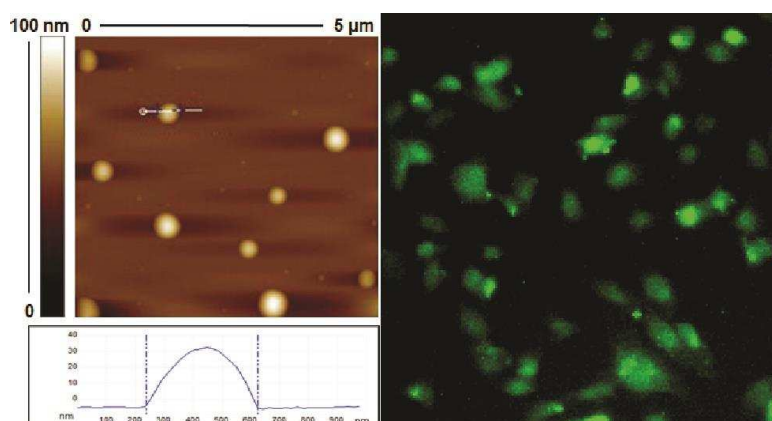
Wenxing Song¹, Munitta Muthana², Joy Mukherjee¹, Robert J. Falconer¹, Catherine A. Biggs¹, Xiubo Zhao^{1*}

¹Department of Chemical and Biological Engineering, University of Sheffield, Mappin Street, Sheffield S1 3JD, UK

²Departments of Infection and Immunity, University of Sheffield, Beech Hill Road, Sheffield S10 2RX, UK

*Author for correspondence: Xiubo Zhao, phone +44 114 222 8256, email:

Xiubo.zhao@sheffield.ac.uk



AFM image of the magnetic-silk core-shell nanoparticles (left) and fluorescent microscopic image (right) of the curcumin delivered human Caucasian breast adenocarcinoma cells.